Microwave Irradiation Controls the Manganese Oxidation States of Nanostructured ($Li[Li_{0.2}Mn_{0.52}Ni_{0.13}Co_{0.13}Al_{0.02}]O_2$) Layered Cathode Materials for High-Performance Lithium Ion Batteries

Charl J. Jafta,[a,b,d] Kumar Raju,[a] Mkhulu K. Mathe,[a,*] Ncholu Manyala,[b] and Kenneth I. Ozoemena[a,c,*,z]

[a]*Energy Materials, Materials Science and Manufacturing, Council for Scientific and Industrial Research (CSIR), Pretoria 0001, South Africa*
[b]*Department of Physics, Institute of Applied Materials, SARChI Chair in Carbon Technology and Materials, University of Pretoria, Pretoria 0002, South Africa*
[c]*Department of Chemistry, University of Pretoria, Pretoria 0002, South Africa*

A hybrid synthesis procedure, combining microwave irradiation and conventional annealing process, is described for the preparation of lithium-rich manganese-rich cathode materials, $Li[Li_{0.2}Mn_{0.54}Ni_{0.13}Co_{0.13}]O_2$ (LMNC) and its aluminum-doped counterpart, $Li[Li_{0.2}Mn_{0.52}Ni_{0.13}Co_{0.13}Al_{0.02}]O_2$ (LMNCA). Essentially, this study interrogates the structure and electrochemistry of these layered cathode materials when subjected to microwave irradiation (these microwave-based produced are abbreviated herein as $LMNC_{\text{-mic}}$ and $LMNCA_{\text{-mic}}$). The nanoparticulate nature of these layered cathode materials were confirmed by SEM. The crystallinity and layeredness were determined from the XRD analysis. The XPS measurements proved a definite change in the oxidation states of the manganese due to microwave irradiation. The galvanostatic charge-discharge characterization showed that the aluminum-doped cathode material obtained with the assistance of microwave irradiation has superior electrochemical properties. In summary, the electrochemical performance of these cathode materials produced with and without the assistance of microwave irradiation decreased as follows: $LMNCA_{mic} > LMNCA > LMNC_{mic} > LMNC$.

With the burgeoning world population and the ever-increasing demand for energy, it comes as no surprise that the world faces an energy crisis with fossil fuels depleting and causing global warming. In an effort to keep up with these demands energy conversion technologies with lithium ion battery research, for energy storage, are at the forefront. The $Li[Li_{0.2}Mn_{0.54}Ni_{0.13}Co_{0.13}]O_2$ (LMNC) is a well-known lithium-rich lithium ion battery cathode material.[1–4] These layered cathode materials are unfortunately still plagued by numerous short comings and new strategies explored are the topic of many research reports. Two of these short comings are the cycling ability and the rate capability.[5,6] It has been accepted a priori that the oxidation state of Mn is 4+ and very unlikely 3+, but this could lead to misinterpretation of data related to layered cathode materials. Interestingly, this was shown not to be the case and that the layered cathode material consists of a mixture of Mn^{3+} and Mn^{4+} in the starting material.[7] It becomes then important to know the ratio in the starting layered cathode material since the average valence number of manganese plays a critical role in the capacity retention and rate capability of the battery.

In a previous study,[8] we demonstrated that doping the LMNC with very small amount of aluminum (i.e., $Li[Li_{0.2}Mn_{0.52}Ni_{0.13}Co_{0.13}Al_{0.02}]O_2$ (LMNCA)) improved the rate capability and cycling stability compared to the standard LMNC. This was attributed to the increased *c* lattice due to Al doping that caused a better Li diffusion. With the minute Al-doping (the same as the present work) there was an increase in the stability but an initial lowered discharge capacity compared to the LMNC. This was explained by the redox-inactive Al. It was also shown from the XPS experiments that the oxidation state of Mn decreases by substituting Mn with Al. In the present work, we introduced microwave irradiation as a strategic step in the synthesis process with a view to observing the impact of microwave irradiation on the physico-chemical properties of these two layered cathode materials (LMNC and LMNCA). We clearly prove that microwave irradiation leads to improved structure and electrochemical performance. Interestingly, contrary to the former finding where the doping with aluminum led to an increase in the Mn^{3+} content, our strategic pre-annealing stage microwave irradiation resulted in the decrease of the Mn^{3+} concentration. In a nutshell, the inclusion of microwave irradiation step in the production process enhances the electrochemical performance of both LMNC and LMNCA in terms of capacity, cyclability/capacity retention, and rate capability.

Most experiments with microwave heating reveal results different from those obtained with conventional heating processes.[9,10] Two main hypotheses underlying the microwave effects are known. The first assumes the existence of a purely thermal effect (i.e. hot spots and temperature gradient) by dipolar polarization and ionic conduction.[11] The second theory assumes that, besides thermal effects there are also non-thermal effects like molecular interaction with the electromagnetic field as shown by Roy et al.[12] It is generally accepted that there are a number of characteristics specific to microwaves as agents for promoting chemical reactions: (i) the quantum energy of microwaves (10^{-5} eV) which is much lower than that of chemical bonds making it improbable for microwaves to break or weaken bonds within molecules; (ii) the intensity of electric and magnetic fields that is unable to cause the shift of any chemical reaction equilibrium.

Generally speaking, the synthesis process for electrode materials for lithium ion batteries involves two main conventional heating stages; (i) the initial pre-heating or calcination stage (usually about 500°C, between 7 and 10 hours), and (ii) annealing stage (≥700°C, between 8 and 36 hours). However, to the best of our knowledge, researchers who have used microwave-assisted synthesis for the preparation of electrode materials have done so with the view of using microwave irradiation as a means of achieving fast heating or annealing process, thereby reducing the synthesis time. This explains why, for example, Balaji et al.[10] in their 'review of microwave synthesis of electrode materials for lithium-ion batteries' observed and rightly concluded that an economical process of synthesizing electrode materials could be the use of microwave radiation as the primary stage of pre-heating/calcination with the conventional high-temperature annealing at a later stage. The aim of our work is not to replace any of the conventional heating stages with microwave heating, as is generally the case with most researchers, but rather to incorporate fast microwave irradiation (∼20 minutes) as a part of the primary pretreatment stage with the view of tuning the physico-chemical properties of the materials. This work presents the first report on this type of microwave treatment on layered cathode materials and proves that the process is capable of positively impacting on the structural and electrochemical integrity of LMNC and LMNCA for lithium ion battery.

*Electrochemical Society Active Member.
[d]Present address: Helmholtz-Zentrum Berlin für Materialien und Energie (HZB), 14109 Berlin, Germany.
[z]E-mail: kozoemena@csir.coza

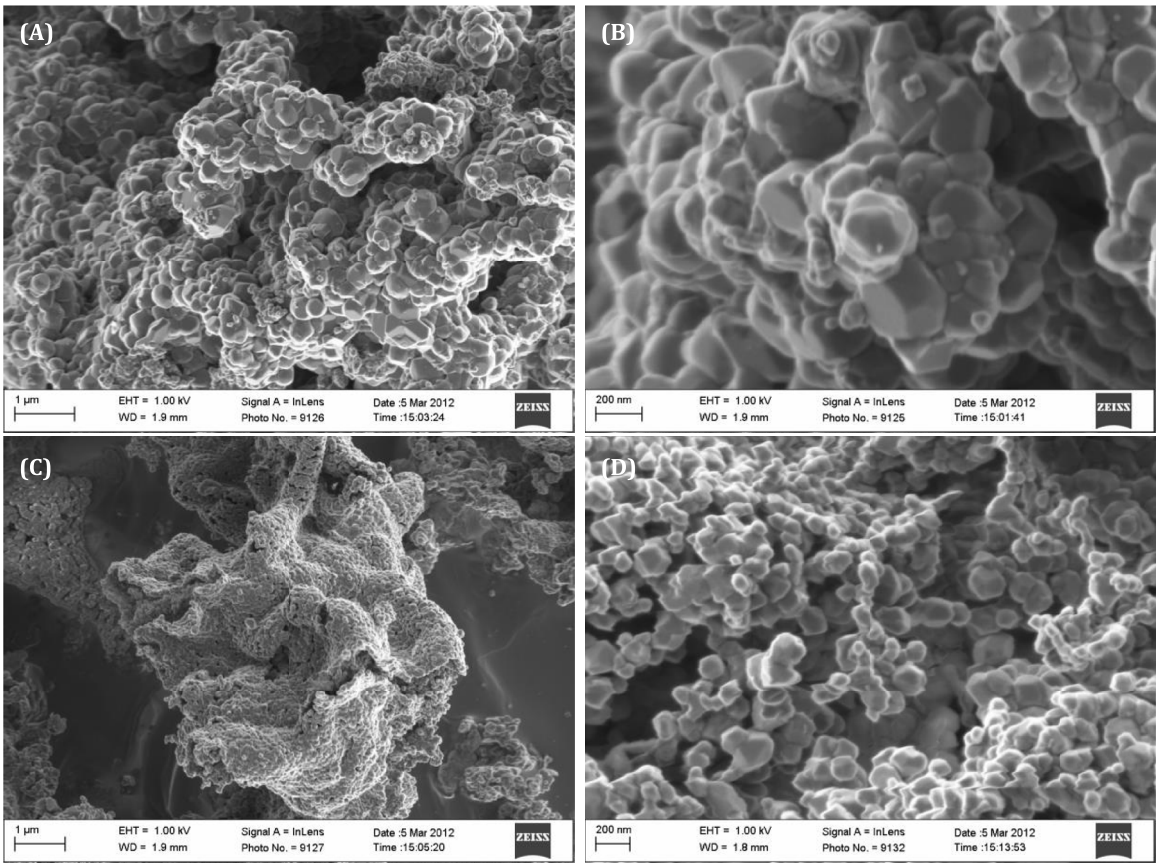

Figure 1. FESEM images of (A) LMNC-mic at low magnification, (B) LMNC-mic at high magnification, (C) LMNCA-mic at low magnification and (D) LMNCA-mic at high magnification.

Experimental

The parent $Li[Li_{0.2}Mn_{0.54}Ni_{0.13}Co_{0.13}]O_2$ (LMNC) and Al-doped $Li[Li_{0.2}Mn_{0.52}Ni_{0.13}Co_{0.13}Al_{0.02}]O_2$ (LMNCA) precursor powder materials were prepared using the modified Pechini method,[8] using citric acid (CA), ethylene glycol (EG) and metal (Li, Ni, Co, Al) nitrates as starting materials. The reducing agent, CA (dissolved in deionized water) and EG was mixed in the ratio 1:4 (CA : EG) and heated at approximately 90°C while constantly stirring for 30 minutes. Stoichiometric amounts of $LiNO_3$, $Ni(NO_3)_2 \cdot 6H_2O$, $Co(NO_3)_2 \cdot 6H_2O$, $Mn(NO_3)_2 \cdot 4H_2O$ and $AlN_3O_9 \cdot 9H_2O$ were dissolved in deionized water and then introduced, drop-wise, to the reducing solution. The solutions were then dehydrated into gels. The gels were kept at a temperature of 90°C until the solutions spontaneously formed the desired powders. The precursor powders (LMNC and LMNCA) were preheated at 500°C for 6 h and each divided into two batches. The one batch was annealed at 700°C for 8 h (LMNC and LMNCA). The other half was irradiated with microwaves ($\lambda = 0.12236$ m), where the power was increased at a rate of 60 W per minute to 600 W and irradiated at this power for 15 min (the temperature of the samples reached a maximum of 60°C) and then annealed at 700°C for 8 h (LMNC-mic and LMNCA-mic).

Results and Discussion

Figures 1A–1D compares the SEM images of LMNC-mic and LMNCA-mic, showing that the synthesized materials comprised of nano-sized particles with sizes in the 250–300 nm range for the LMNC-mic (see Figure 1A and 1B), and 100–200 nm range for the LMNCA-mic (see Figures 1C and 1D). These particle sizes are comparable to the un-microwaved samples with sizes in the 50–100 nm range for the LMNC, and 50–200 nm range for the LMNCA.[8]

Figure 2 shows the XRD spectra of the LMNC-mic and LMNCA-mic recorded from $2\theta = 10°$–$90°$. All the peaks are attributed to the typical peaks of a hexagonal phase with space group $R\bar{3}m$. Also, the XRD patterns showed weak peaks around 21.8° (Fig. 2 inset) which can be attributed to the superlattice structure of Li_2MnO_3, which by contrast adopts the C2/m space group.[13–15] The intensity ratio of the 101/(006 + 102) peaks are greater than 2 which is an indication that the cation mixing between Li and transition metal layers is small.[16] The lattice parameters, *a* and *c*, were calculated

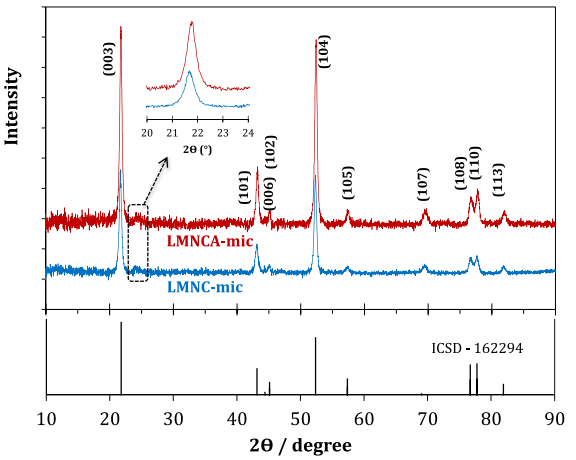

Figure 2. XRD patterns of LMNC-mic ($Li[Li_{0.2}Mn_{0.54}Ni_{0.13}Co_{0.13}]O_2$) and LMNCA-mic ($Li[Li_{0.2}Mn_{0.52}Ni_{0.13}Co_{0.13}Al_{0.02}]O_2$). The inset is the zoomed portion of the peaks due to the superlattice structure of Li_2MnO_3.

Table I. Structure parameters of the LMNC and LMNCA samples.

Sample	*a* (Å)	*c* (Å)	*c*/*a*
LMNC-mic	2.852 ± 0.057	14.216 ± 0.284	4.985 ± 0.100
LMNC	2.852 ± 0.057	14.173 ± 0.081	4.970 ± 0.100
LMNCA-mic	2.846 ± 0.057	14.233 ± 0.284	5.001 ± 0.100
LMNCA	2.853 ± 0.057	14.238 ± 0.285	4.990 ± 0.100

using the Rietveld and least squares methods and are summarized in Table I.

The lattice parameters *a* and *c* represent the interlayer metal-metal distance and the inter-slab distance, respectively. It is known that Li ions in addition to the transition metals are found in the predominantly transition metal layers and vice versa, which is termed cation disorder. By decreasing the cation disorder, the diffusion of Li is increased. The LMNCA-mic has a higher *c*/*a* ratio, indicating a higher cation ordering compared to the LMNC-mic. There is no significant change in the *a* lattice parameter but a slight increase in the *c* lattice parameter when doped with a minute amount of Al (x = 0.02) which may be attributed to the increased ionic radius of Al^{3+} ($r(Al^{3+}) = 53.5$ pm)[17] compared to the smaller ionic radius of Mn^{4+} ($r(Mn^{4+}) = 53.0$ pm).[18] Also, the increase in the *c* lattice parameter, in layered materials, is associated with faster Li diffusion due to the decrease in the activation energy of Li hopping.[19] Again, the LMNCA-mic shows a greater *c* lattice and thus faster Li diffusion is expected that would result in better rate capability compared to the cathode materials LMNC, LMNCA and LMNC-mic. The *c*/*a* ratio is an indication of the hexagonal setting, with a larger ratio indicating higher cation ordering. Partial cation mixing is said to occur if the *c*/*a* ratio falls below 4.96.[20–24] The *c*/*a* ratios obtained for all the samples clearly confirm the formation of the layered structures for both the microwave-treated and standard samples.

Figure 3 shows the detailed XPS spectra of the Mn $2p_{3/2}$ peaks of the LMNC-mic (Figure 3A) and LMCA-mic (Figure 3B).

There is a broadening in both the peak widths, an indication that the Mn exist in more than one oxidation state. In order to confirm the oxidation states and to approximate their contribution to the total peak, the Mn $2p_{3/2}$ of the LMNC and the LMNCA peaks were deconvoluted into two and three peaks, respectively, as this gives the best statistical fit. The third peak ('sat') observed from the LMNC-mic is a satellite peak usually ascribed to an electron hole, with a relatively longer life-time, created in the core levels.[8] The obtained binding energy positions and cation distribution are summarized in Table II.

The binding energy peak positions corresponding to Mn^{4+} and Mn^{3+} are comparable with other binding energy values reported in the literature.[24,25] The microwaved materials show slightly higher average Mn valence number compared to their corresponding un-microwaved materials (i.e., LMNC-mic > LMNC, and LMNCA-mic > LMNCA). The higher oxidation state of manganese with microwave radiation is also observed by Malinger et al.[26] It has recently been shown that the rapid transformation of layered $LiMnO_2$ to spinel is due to the ease at which Mn^{3+} disproportionate to Mn^{2+} and Mn^{4+}.[27] This then allows the Mn to rapidly move through tetrahedral sites as Mn^{2+}. Mn^{4+}, however, has a very high activation energy barrier for diffusion through tetrahedral sites. Therefore layered materials with a higher oxidation state for their manganese are expected to be more stable

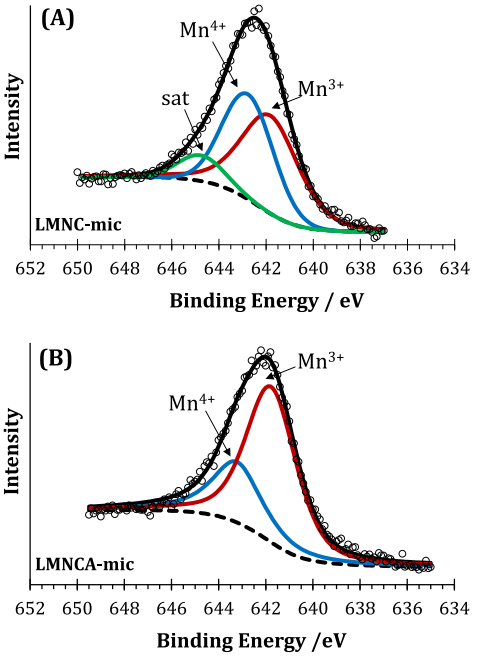

Figure 3. The X-ray Photoelectron Spectroscopy spectra of (A) LMNC-mic and (B) LMNCA-mic, showing the Mn $2p_{3/2}$ peak.

as seen in this study. Also the specific capacity of Li-rich layered cathode materials can be controlled by controlling the initial ratio of transition metal cations, particularly lithium and manganese ions.[28] This method of synthesizing $Li[Li_{0.2}Mn_{0.54}Ni_{0.13}Co_{0.13}]O_2$ and the Al-doped $Li[Li_{0.2}Mn_{0.52}Ni_{0.13}Co_{0.13}Al_{0.02}]O_2$ thus provides an opportunity to control the Mn oxidation state and thus engineer a cathode material with better properties.

Figure 4 compares the first charge-discharge profiles of the four layered materials (LMNC, LMNCA, LMNC-mic and LMNCA-mic) used in coin cells at a rate of C/10 (i.e., ~22.5 $mA.g^{-1}$, note that 1 C corresponds to 225 $mA.g^{-1}$ current density in this work).

Both electrodes show similar charge profiles with a prolonged voltage plateau at ~4.5 V. The charge curve shapes are explained in detail in Ref. 5. The LMNCA-mic showed a higher charge capacity of ~375 $mAh.g^{-1}$ compared to the LMNC-mic with a charge capacity of ~270 $mAh.g^{-1}$. This was also observed for the un-microwaved samples where the LMNCA had a higher charge capacity than the LMNC.[5] The LMNCA-mic also has a higher first discharge capacity of ~278 $mAh.g^{-1}$ compared to the LMNC-mic with a discharge capacity of ~224 $mAh.g^{-1}$.

Figure 5 compares the cycle stability at a rate of C/10 for 50 discharge cycles of the four layered materials (LMNC, LMNCA, LMNC-mic and LMNCA-mic) used in coin cells when charged between 2.0 V and 4.8 V.

During the first 6 cycles these microwave treated samples showed unstable discharge capacities. This behavior may be related to possible relaxation processes, or due to insufficient wetting of the electrode materials, or a combination of the two. Detailed studies are necessary to understand this behavior and improve the stability of the first

Table II. Mn $2p_{3/2}$ peak positions and cation distribution of LMNC and LMNCA based layered materials.

	Binding energy position(eV)		Cation distribution			Mn valence
Sample	Mn^{4+}	Mn^{3+}	Mn^{4+}	Mn^{3+}	Mn^{3+}/Mn^{4+}	Mn^{n+}
LMNC-mic	642.8	641.8	44.9%	55.1%	1.227	3.449
LMNC	643.2	641.8	31.6%	68.4%	2.165	3.316
LMNCA-mic	643.2	641.8	30.8%	69.2%	2.247	3.308
LMNCA	643.1	641.7	18.2%	81.6%	4.484	3.176

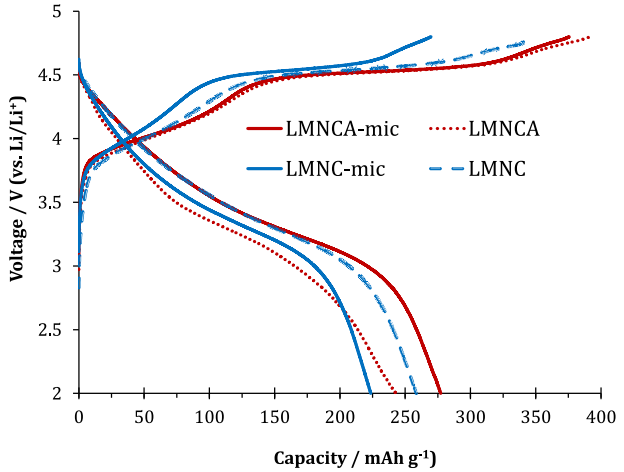

Figure 4. The first charge-discharge profiles of the four LMNC and LMNCA based coin cells.

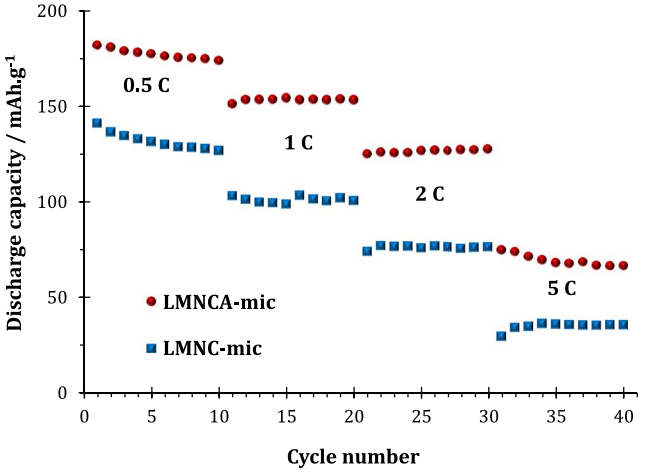

Figure 6. Typical rate capability of the LMNC-mic and LMNCA-mic, charged and discharged at 0.5 C, 1 C, 2 C and 5 C.

charge-discharge cycles. From the 7th cycle the discharge capacities starts to stabilize. The first 6 discharge capacities for LMNCA-mic vary between ca. 270 and 220 mA.h.g^{-1}, while LMNC-mic vary between and 265 and 230 mA.h.g^{-1}. It is worth noting that even though the LMNC-mic material has a better capacity at first, the LMNCA-mic shows a higher capacity from the 28th cycle due to its better stability. Because Al is electrochemically inactive, it is expected that the capacity of the Al doped cathode material (LMNCA-mic) to show a lower discharge capacity. This reduced discharge capacity with Al-doping is also observed in the in the paper from Wilcox et al.[29] It is also worth noting that after 50 charge-discharge cycles, the microwave-treated materials (LMNC-mic and LMNCA-mic) were able to retain about 78% of their initial capacity compared to the standard materials (LMNC and LMNCA) that retained about 60% of their initial capacity. The increased capacity and enhanced capacity retention of the microwave-treated samples suggest a combined effect of microwave irradiation and aluminum-doping.

Considering the high performance of the microwave-treated samples, their rate capabilities were investigated. Figure 6 compares the rate capabilities of the LMNC-mic and LMNCA-mic at charge and discharge rates of 0.5, 1, 2 and 5 C. With the XRD data showing that LMNCA-mic has a bigger *c* lattice parameter compared to LMNC-mic it is thus expected that LMNCA-mic would have a better rate capability. As seen from Figure 6 this is indeed the case. The *c* lattice is not the only factor responsible for high rate capability; the concentration

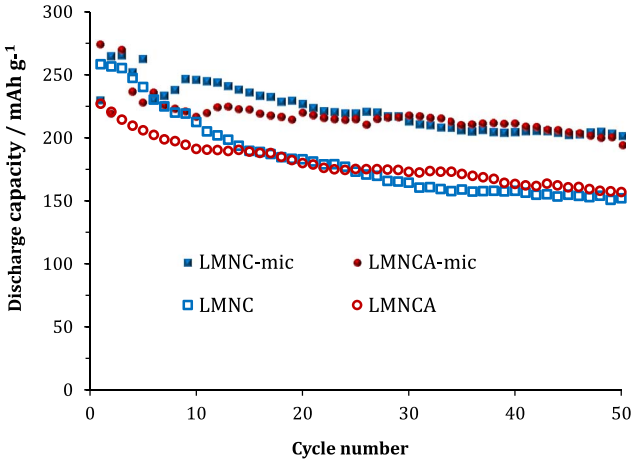

Figure 5. The cycle stability of the four LMNC and LMNCA based coin cells at C/10 for 50 charge discharge cycles.

of Mn^{3+} will increase the electron conductivity and better the rate capability. The microwave-treated material with the higher *c*-lattice parameter and higher Mn^{3+} concentration (LMNCA-mic) gave better rate capability. Thus, it is deduced that a good combination of the two (*c* lattice and Mn^{3+} concentration) is needed for high rate capability.

Figure 7 shows the cyclic voltammetric evolutions of LMNC-mic and LMNCA-mic. The initial and second cycle of the LMNC-mic and LMNCA-mic is interrogated using low scan rate cyclic voltammetry (0.1 mV.s^{-1}). Again, the cyclic voltammograms of the LMNC and LMNCA, that are similar to LMNC-mic and LMNCA-mic, are discussed in detail in Ref. 8. The peaks at ~4.7 V, for both LMNC-mic and LMNCA-mic, of their initial cycles disappear with the 2nd cycle showing the irreversible removal of Li_2O. With the higher peak current at ~4.7 V for the LMNCA-mic, the higher first charge of the LMNCA-mic compared to the LMNC-mic can be explained (see Figure 4). Thus it can be assumed that the microwave irradiation in the LMNCA-mic causes more oxygen vacancies and therefore result in a higher concentration of Li_2O being removed.

Electrochemical impedance spectroscopy (EIS) represents an important technique for evaluating interfacial electrochemistry[30–33] and diffusion coefficient of lithium ion in lithium ion battery materials.[34–36] The impedance spectra for the LMNC-mic and LMNCA-mic were measured at a potential of 3.5 V. The spectra were recorded before the 1st cycle (Figure 8A) and after the 50th cycle (Figure 8B). Prior to every measurement, the cell was relaxed for 1 h. Figure 8 presents typical Nyquist plots (Z′ vs –Z″) obtained for the LMNC-mic and LMNCA-mic cells. A high-frequency semicircle and an intermediate-frequency semicircle composed into one semi-circle, and low frequency tails are observed. Generally, the high frequency semicircle is related to the passivating surface film, the solid-electrolyte interface (SEI). The intermediate frequency semicircle is ascribed to the resistance to charge-transfer process at the electrode/electrolyte interface. The low frequency tail is associated with the Li^+ ion diffusion process in the positive electrode. The EIS spectra were fitted with an equivalent electrical circuit (EEC) shown in Figure 8A (as an inset). The fitting parameters involve the solution *ohmic* resistance of the electrode system (R_s), solid electrolyte interface (SEI) film resistance (R_f), charge transfer resistance (R_{ct}) due to lithium intercalation/de-intercalation process, the capacitance of the surface film (C_f) and the interfacial capacitance (C_{Li}), and the Warburg element (Z_w) describing the solid state diffusion of lithium ions inside the active particles, signified by the straight sloping line (~45°) at the low frequency region.

The EIS parameters obtained for the LMNC-mic and LMNCA-mic are summarized in Table III. After 50 cycles, the R_f value for LMNCA-mic decreased by about 80% (from 3.14 to 6.2 Ω) but the standard LMNCA decreased by about 77% (from 536 to 123 Ω), the

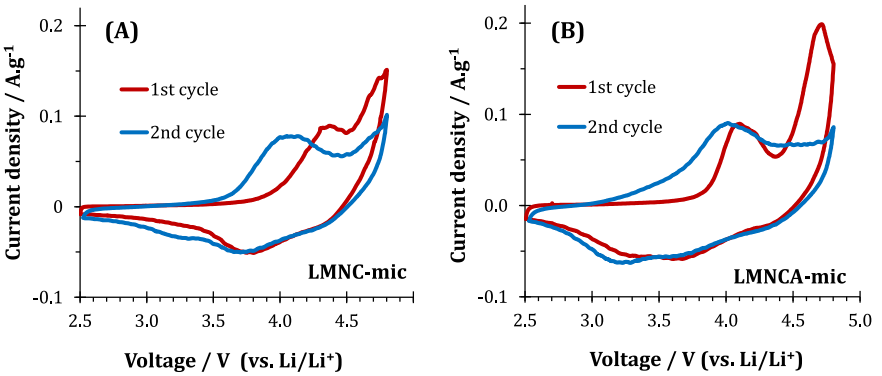

Figure 7. The cyclic voltammograms of (a) LMNC-mic and (b) LMNCA-mic obtained at a scan rate of 0.1 $mV.s^{-1}$ (first and second cycles).

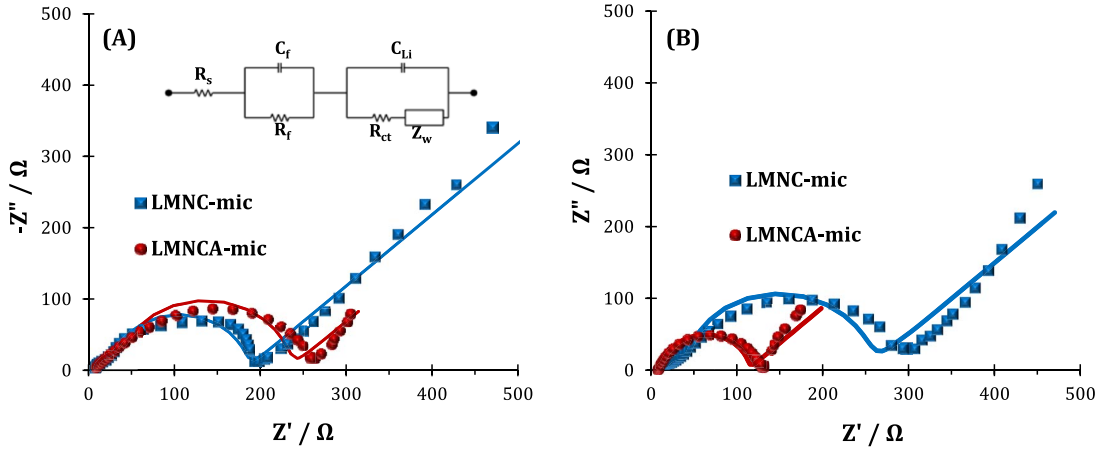

Figure 8. Comparative Nyquist plots of LMNC-mic and LMNCA-mic (a) before the 1st cycle and (b) after 50 cycles.

LMNC-mic increased by about 20% (from 22.4 to 26.7 Ω), while that of the standard LMNC increased by well over 1300% (from 11.1 to 159 Ω). On the other hand, for the R_{Li}, after 50 cycles, the value for the LMNCA-mic decreased by about 50% (from ca. 192 to 98 Ω), but the LMNCA decreased by about 50% (from ca. 246 to 124 Ω), the LMNC-mic increased by about 35% (from ca. 153 to 207 Ω), while that of the LMNC increased by about 73% (from ca. 117 to 203 Ω).

In summary, the conductivity of these layered materials decreases as follows: $LMNCA_{mic}$ (Mn^{3+} content: 69.2%) > LMNCA (Mn^{3+} content: 81.6%) > $LMNC_{mic}$ (Mn^{3+} content: 55.1%) > LMNC (Mn^{3+} content: 68.4%). The enhanced conductivity of the LMNCA may be related to its higher Mn^{3+} content in the lattice, aided by the improved *c*-lattice that enhances the diffusivity of Li during the electrochemical cycling. In summary, these results suggest that the following: (i) the possible mitigating factor for R_f is more of aluminum-doping than microwave irradiation; (ii) the effect of microwave irradiation is most pronounced for the undoped LMNC than the Al-doped samples; and (iii) that the electrochemical performance is a combination effect of microwave irradiation and aluminum-doping. The main consequences of the solid-electrolyte interphase (SEI) are the increased interfacial resistance and loss of active material.[34] From the R_{ct} and R_f values it can be deduced that the SEI film covering the LMNCA-based electrode surface is rapidly destroyed, or replaced by redox-active active material, or that the SEI layer has been stabilized by a lithium-ion conducting (non-redox-active) species upon continuous cycling. For the LMNC-based materials, however, there seems to be some SEI growth and/or loss of active materials hence poor lithium ion diffusion upon continuous cycling. The apparent diffusion coefficient of lithium ions (D_{Li}) was calculated by means of Equation 1:[8]

$$D_{Li} = \frac{2R^2T^2}{C_{Li}^2 n^4 F^4 A^2 \sigma^2} \quad [1]$$

Assuming diffusion coefficients of the oxidized and reduced Li species to be equal ($D_{ox} = D_{red} = D_{Li}$) and equal concentrations ($C_{ox} = C_{red} = C_{Li}$). D_{Li} is the diffusion coefficient of the lithium ions, R the gas constant, T the absolute temperature, A the geometric surface area

Table III. Summary of EIS parameters extracted from the Nyquist plots from experiment conducted at 3.5 V.

Sample	R_s (Ω)	R_f (Ω)	C_f (μF)	C_{Li} (μF)	R_{Li} (Ω)	Z_w ($\times 10^{-4}$)
Before cycling						
LMNC-mic	7.0 ± 0.5	22.4 ± 2.2	0.7 ± 0.1	2.4 ± 0.2	152.6 ± 5.4	83.5 ± 4.6
LMNCA-mic	9.0 ± 0.6	31.4 ± 2.7	0.5 ± 0.0	2.2 ± 0.2	191.6 ± 7.2	80.2 ± 13.2
LMNC[8]	9.6 ± 0.4	11.1 ± 1.1	1.2 ± 0.1	3.5 ± 0.2	117.3 ± 2.7	234.5 ± 23.5
LMNCA[8]	3.9 ± 0.4	536.0 ± 24.6	174.5 ± 29.0	8.3 ± 0.7	245.6 ± 19.3	224.6 ± 70.5
After 50 cycles						
LMNC-mic	16.1 ± 1.3	26.7 ± 2.5	0.4 ± 0.1	2.5 ± 0.2	206.8 ± 9.0	48.7 ± 2.9
LMNCA-mic	8.1 ± 0.5	6.2 ± 1.5	1.9 ± 0.5	2.4 ± 0.2	98.2 ± 3.4	146.5 ± 8.7
LMNC[8]	8.0 ± 0.4	158.8 ± 15.5	252.1 ± 69.0	6.6 ± 0.4	202.6 ± 11.2	150.1 ± 13.1
LMNCA[8]	8.2 ± 0.4	123.2 ± 12.2	124.2 ± 44.9	5.4 ± 0.6	123.6 ± 11.4	101.4 ± 5.4

of the cathode, F the Faraday constant, n the number of electrons transferred per molecule during oxidation, C_{Li} the lithium concentration in the cathode material and σ is the Warburg factor obtained from the slope of the real impedance (Z') vs. the reciprocal square root of the frequency in the low frequency region ($\omega^{-1/2}$) according to Eq. 2 (plot not shown).

$$Z_w = \sigma\,(1 - j)\,\omega^{-1/2} \qquad [2]$$

As expected, the calculated diffusion coefficient value for LMNC-mic of $1.59 \pm 0.24 \times 10^{-13}$ $cm^2.s^{-1}$ is inferior to the value for LMNCA-mic of $2.01 \pm 0.29 \times 10^{-13}$ $cm^2.s^{-1}$.

Conclusions

A microwave-assisted Pechini synthesis method has been used to prepare nanostructured layered cathode materials for lithium ion batteries, $Li[Li_{0.2}Mn_{0.54}Ni_{0.13}Co_{0.13}]O_2$ and $Li[Li_{0.2}Mn_{0.52}Ni_{0.13}Co_{0.13}Al_{0.02}]O_2$. The precursor powder materials were first produced by sol-gel like process (Pechini method), then pre-heated, and subjected to microwave irradiation prior to conventional annealing process. This hybrid synthesis method showed that the oxidation states of the manganese can be controlled by doping LMNC with Al and microwave irradiation treatment. The $LMNCA_{mic}$ outperforms the $LMNC_{mic}$ and ultimately is superior compared to LMNC, LMNCA. From the electrochemical performance of these cathode materials that decreased as follows: $LMNCA_{mic} > LMNCA > LMNC_{mic} > LMNC$, it can be concluded that both Al-doping and microwave irradiation can be used to tune to the electrochem-ical performance of these layered cathode materials for lithium ion batteries.

Acknowledgments

This work was funded by the CSIR as well as the South Africa's Department of Science and Technology (DST) and National Research Foundation (NRF) under the *"Nanotechnology Flagship Programme"* (Grant No: 69849). CJJ thanks the CSIR for doctoral studentship.

References

1. M. M. Thackeray, C. S. Johnson, J. T. Vaughey, N. Li, and S. A. Hackney, *J. Mater. Chem.*, **15**, 2257 (2005).
2. M. M. Thackeray, S.-H. Kang, C. S. Johnson, J. T. Vaughey, and S. A. Hackney, *Electrochem. Commun.*, **8**, 1531 (2006).
3. C. S. Johnson, N. Li, C. Lefief, and M. M. Thackeray, *Electrochem. Commun.*, **9**, 787 (2007).
4. S.-H. Kang, P. Kempgens, S. Greenbaum, A. J. Kropf, K. Amine, and M. M. Thackeray, *J. Mater. Chem.*, **17**, 2069 (2007).
5. S. J. Shi, J. P. Tu, Y. Y. Tang, X. Y. Liu, X. Y. Zhao, X. L. Wang, and C. D. Gu, *J. Power Sources* **241**, 186 (2013).
6. M. Iftekhar, N. E. Drewett, A. R. Armstrong, D. Hesp, F. Braga, S. Ahmed, and L. J. Hardwick, *J. Electrochem. Soc.* **161**, A2109 (2014).
7. L. Simonin, J.-F. Colin, V. Ranieri, E. Can´evet, J.-F. Martin, C. Bourbon, C. Baehtz, P. Strobel, L. Daniel, and S. Patoux, *J. Mater. Chem.* **22**, 11316 (2012)
8. C. J. Jafta, K. I. Ozoemena, M. K. Mathe, and W. D. Roos, *Electrochim. Acta*, **85**, 411 (2012).
9. W. Tu and H. Liu, *J. Mater. Chem.*, **10**, 2207 (2000).
10. S. Balaji, D. Mutharasu, N. Sankara Subramanian, and K. Ramanathan, *Ionics*, **15**, 765 (2009).
11. C. O. Kappe, *Chem. Soc. Rev.*, **37**, 1127 (2008).
12. R. Roy, R. Peelamedu, L. Hurtt, J. Cheng, and D. Agrawal, *Mater. Res. Innov.*, **6**, 128 (2002).
13. M. M. Thackeray, S. Kang, C. S. Johnson, J. T. Vaughey, R. Benedek, and S. Hackney, *J. Mater. Chem.*, **17**, 3112 (2007).
14. H. Deng, I. Belharouak, Y. Sun, and K. Amine, *J. Mater. Chem.*, **19**, 4510 (2009).
15. G. M. Koenig Jr., I. Belharouak, H. M. Wu, and K. Amine, *Electrochim. Acta*, **56**, 1426 (2011).
16. J. N. Reimers, W. Li, and J. Dahn, *Phys. Rev. B*, **47**, 8486 (1993).
17. J. Krok-Kowalski, J. Warczewski, E. Malicka, T. Gron, H. Duda, T. Mydlarz, M. Pawelczyk, A. Pacyna, P. Rduch, and G. Wladarz, *Proceedings of the XXXVIII International School and Conference on the Physics of Semiconductors, "Jaszowiec", ThP46, 201* (2009).
18. D. Varshney, M. Shaikh, N. Dodiya, and I. Mansuri, *AIP Proceedings*, **1349**, 155 (2011).
19. K. Kang, Y. S. Meng, J. Breger, C. P. Grey, and G. Ceder, *Science*, **311**, 977 (2006).
20. Y. Choi, S. Pyun, and S. Moon, *Solid State Ionics*, **89**, 43 (1996).
21. S. Gopukumar, Y. Jeong, and K. B. Kim, *Solid State Ionics*, **159**, 223 (2003).
22. M. S. Whittingham, *Chem. Rev.*, **104**, 4271 (2004).
23. Z. Lu, D. MacNeil, and J. Dahn, *Electrochem. Solid-State Lett.*, **4**, A200 (2001).
24. K. M. Shaju, G. V. Subba Rao, and B. V. R. Chowdari, *Electrochim. Acta*, **48**, 145 (2002).
25. T. Yi and X. Hu, *J. Power Sources*, **167**, 185 (2007).
26. K. A. Malinger, K. Laubernds, Y. C. Son, and S. L. Suib, *Chem. Mater.*, **16**, 4296 (2004).
27. J. Reed, G. Ceder, and A. Van Der Ven, *Electrochem. Solid-State Lett.*, **4**, A78 (2001).
28. S. H. Yu, T. Yoon, J. Mun, S. Jin Park, Y. S. Kang, J. H. Park, S. M. Oh, and Y. E. Sung, *J. Mater. Chem. A*, **1**, 2833 (2013).
29. J. D. Wilcox, E. E. Rodriguez, and M. M. Doeff, *J. Electrochem. Soc.*, **156**, A1011 (2009).
30. M. E. Orazem and B. Tribollet, *Electrochemical impedance spectroscopy*, John Wiley & Sons, New Jersey, 2011.
31. S. A. Mamuru, K. I. Ozoemena, T. Fukuda, and N. Kobayashi, *J. Mater. Chem.*, **20**, 10705 (2010).
32. K. I. Ozoemena, N. S. Mathebula, J. Pillay, G. Toschi, and J. A. Verschoor, *Phys. Chem. Chem. Phys.*, **12**, 345 (2010).
33. J. Pillay, K. I. Ozoemena, R. T. Tshikhudo, and R. M. Moutloali, *Langmuir*, **26**, 9061 (2010).
34. H. Xia and L. Lu, *Phys. Scripta*, **2007**, 43 (2007).
35. K. Shaju, G. S. Rao, and B. V. R. Chowdari, *J. Electrochem. Soc.*, **151**, A1324 (2004).
36. K. Dokko, M. Mohamedi, M. Umeda, and I. Uchida, *J. Electrochem. Soc.*, **150**, A425 (2003).
37. M. B. Pinson and M. Z. Bazant, Theory of SEI Formation in Rechargeable Batteries: Capacity Fade, Accelerated Aging and Lifetime Prediction (2012).